POAC'15
Trondheim, Norway

Proceedings of the 23rd International Conference on
Port and Ocean Engineering under Arctic Conditions
June 14-18, 2015
Trondheim, Norway

ANALYSIS OF LOCAL ICE LOAD SIGNALS MEASURED ON AN ARCTIC VOYAGE IN 2013

Jong-Hyun Lee [1], Mi-Ran Hwang [1], Seong Wook Kwon [1], Jeong-Goo Kang [1],
Hee-Mun Park [1], Kyungsik Choi [2], Tak-Kee Lee [1]
[1] Gyeongsang National University, Tongyoung, KOREA
[2] Korea Maritime and Ocean University, Busan, KOREA

ABSTRACT

The aim of this paper is to identify time histories of ice-induced loads and to investigate the characteristics of the signal of a local ice load acting on the side shell in the bow thruster room of an icebreaker in the Arctic Ocean, which was caused by broken ice. The Korean icebreaking research vessel, the "Araon" embarked on a research voyage to the Arctic Ocean during August and September 2013. The measurements of the local ice load were carried out using 25 strain gauges, which included three single gauges. In this study, time histories of the measured signals were analyzed and classified into five types. The characteristic values, including rising time and half-decaying time, were presented.

INTRODUCTION

The icecap in the Arctic Ocean has been shrinking year by year. Consequently, marine transportation through the Northern Sea Route from East Asia to Europe has increased. The ships that navigate through these ice-covered waters are subject to ice loads caused by the sea ice. Ice loads may be conveniently categorized as local ice loads and global ice loads, which generate typically vertical bending moments on the hull girder (ABS, 2011). In particular, local ice loads are often defined as ice pressure that acts on local areas of the ship's structures. They are known to depend on ice type, ice thickness, ice-structure interaction, and dominant ice failure modes (ISSC, 2012).

In severe cases, ice-going ships are subject damage caused by local ice loads due to contact with and the impact of sea ice, as shown in Fig. 1 (Gagnon & Wang, 2012, Republic of Liberia, 2009). The causes of these accidents have been reported to be the effects of collisions with icebergs or the sharp parts of icebergs. However, given the nature of ice-going ships which are unavoidably subject to frequent contact with and impact by sea ice, small damage to the outer hull panel which has been weakened because interactions with sea ice, might be the initial cause of severe accidents.

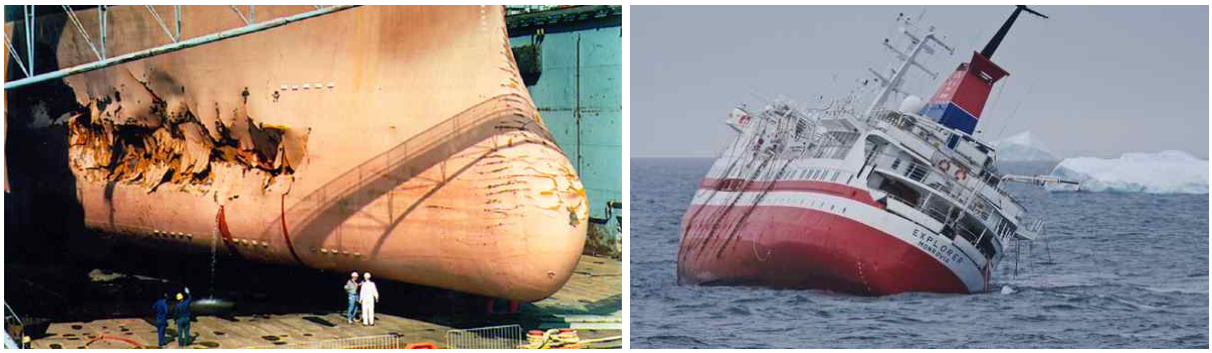

(a) Reduta Ordona (B/C, Photo: A. Kendrick) (b) MS Explorer (Cruiser, wildlifeimages.net)

Figure 1 Examples of damage due to ice collision

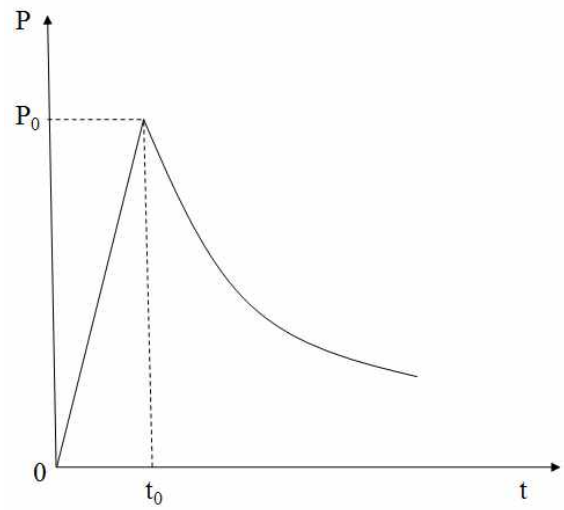

Figure 2 Idealized impulsive pressure history.

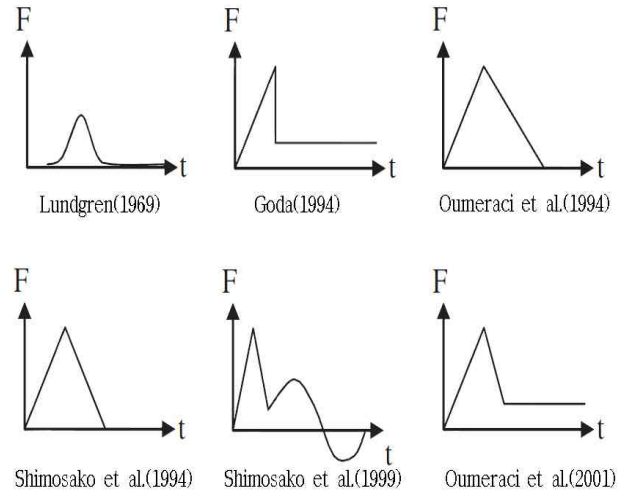

Figure 3 Several wave impact-time history models against caisson breakwaters

To identify the phenomenon of ships impacted by sea ice and their response characteristics, it is necessary to understand the time history during which ice loads are imposed on hull structures (Paik et al., 1999). Fluid impact pressure acts on ships, which include slamming, sloshing, and green sea, can be idealized as shown in Fig. 2. In this case, although the pressure reaches the maximum value in a very short time, it dissipates in the form of an exponential function. When a fluid inflows for a certain period, there is a long tail part in which relatively low pressure is maintained in some cases. This impact of the fluid pressure type is specified by four variables: 1) the time to reach the maximum pressure (rising time); 2) maximum pressure; 3) the form of extinction; and 4) duration of pressure. Cuomo et al. (2011) reviewed several models of the time histories of impulses and semi-static wave loads that act on caisson breakwaters. These models are intended to analyze dynamic stress, initial impact loads, and the subsequent semi-static loads.

Previous studies (Jeon et al., 2013; Kwon et al., 2014) analyzed local ice load data that were measured in 2010 in the Beaufort Sea using the Araon, which is a South Korean icebreaking research vessel. Jeon et al. (2013) analyzed unique types of ice load data that were measured when the icebreaker had ice sea-trials in the Arctic Ocean. They identified that many ice load patterns had one or two peak stages before reaching the maximum. The intervals were

approximately three times longer on average in reaching the maximum pressure, which is an important variable in analysis of characteristics. In addition, Kwon et al. (2014) analyzed the impact history based on paper data from a previous ice load analysis (Lee et al., 2014). Among the data gathered over 6.5 hours (23,400sec.) during general operation, not an ice trial, they examined types of ice load data for 91 stresses exceeding 50 MPa. They divided the ice load patterns into five types, based on whether the data type had intermediate peaks or not.

The present study analyzed the time history of the ice loads measured during the 2013 Arctic voyage of Araon, the same ship that was used in the 2010 study. Focusing on the data from 26 August 2013 when the Araon sailed in ice-covered waters, the ice load data was measured for approximately 38.7 hours (139,320 seconds). The data were measured by strain gauges attached inside the port side shell of the bow thruster room. These data were converted into stresses, and pattern analyses were conducted on 265 cases where the stress peak values exceeded 50 MPa.

Overview of the ice load measurements in the Arctic Ocean in 2013

During the measurement period, the average draft of the Araon was approximately 6.8m. The principal particulars are shown in Table 1 (Kim et al., 2011). Fig. 4 and Table 2 show a view of the Araon under sail, an example of the sea ice conditions, measuring sites on the map, estimated ice concentration, and so on.

Table 1 Principal particulars of the Araon

Length, O.A. (m) / B.P. (m)	111.0 / 95.0
Beam, Maximum WL (m)	19.0
Design Draft / Summer Max. (m)	6.8 / 7.6
Gross Tonnage (ton)	7,487
Speed (knots, 7,500kW)	16.0
Operation Range (naut. Miles)	20,000
Ship Class	Korean Register PL10
Ice Performances (Design Target)	Speed 3knots in 1m level ice with flexural strength of not less than 630kPa

Table 2 Summary of measurements and ice concentration in Araon's Arctic voyage in 2013

Date-time	Measuring site	Measuring time (sec)	No. of peak over 50 MPa	Estimated ice concentration
0826-0328	7532.791N-15853.69W ~ 7608.23N-16026.05W	14,400	22	1-3
0826-0728	7608.23N-16026.05W ~ 7700.12N-16243.2W	36,000	56	4-6
0826-1740	7700.306N-16243.67W ~ 7728.42N-16407.28W	18,000	55	7, 8
0828-1016	7729.778N-17118.52W ~ 7702.38N-17457.84W	28,800	68	4-6
0829-0115	7701.76N-17515.42W ~ 7648.97N-17858.93W	21,600	33	4-6
0830-0300	7625.89N-17852.8W ~ 7602.10N-17942.65W	20,600	31	4-6
Sum		139,400	265	

(a) The Araon in 2013 (Aug. 27, Yonhap News) (b) Ice conditions in the summer of 2013

Figure 4 Views of the Araon and ice conditions

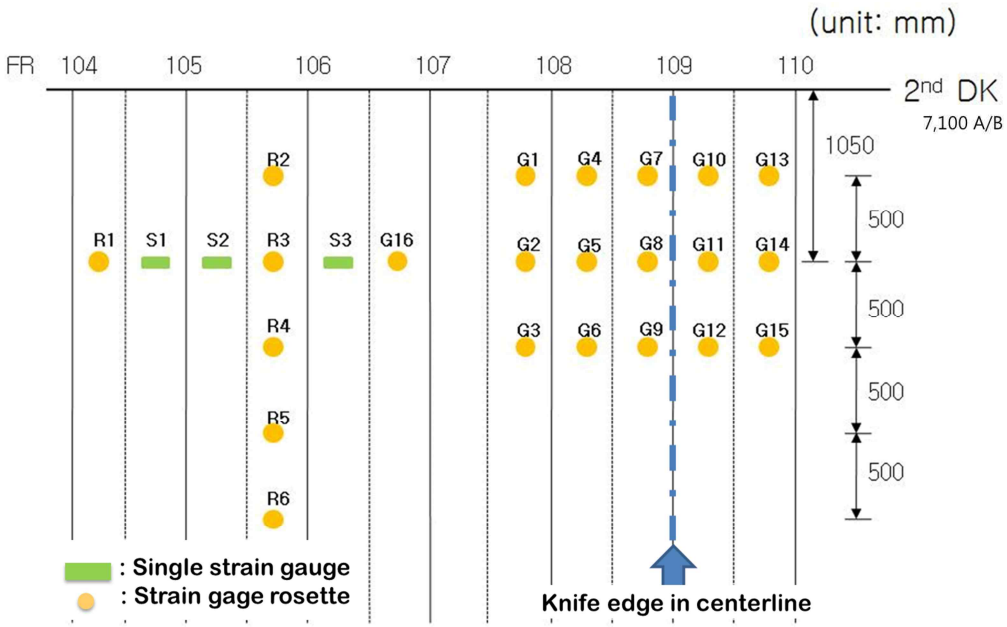

Figure 5 Location of strain gauges during the Arctic voyage in 2013

To measure the local ice load, strain gauges were attached to the inside of the portside in the bow thruster room, as shown in Fig. 5. In this case, S1~S3, R1~R6 gauges were the same as those used during the 2010 Arctic voyage of the Araon. The connection of the strain gauges applied to the measurement was constructed as a half bridge after performing temperature compensation using dummy gauges. The signals measured at a sampling rate of 50Hz, and noises in measuring were removed by applying Bessel low pass filters set to a cut-off frequency of 5Hz.

Analysis of ice load signals during the 2013 Arctic voyage of the Araon

In their analysis of the local ice load signal measured during general operation of the Araon in 2010, Kwon et al. (2014) classified the data into five types, based on whether the data had intermediate peaks or not. The results of the classification of 265 data measured in 2013 based on these criteria were; Type I: 188, Type II: 28, Type III: 35, Type IV: 10, and Type V: 4.

Analysis of the characteristics of ice load data types

The rising time and the half-decaying time of all peak data were summarized according to the type of signal, as shown in Table 3. In the case of signals in Type I, which were the largest number, the average of the two types of time variables showed a smaller value compared to the average of all data. In the case of the signals in Type II, the rising time increased by 0.038 seconds on the average of all data because of the intermediate peaks found in the rising time. However, the half-decaying time was similar as those in the case of Type I, which indicates the effects of the intermediate peaks. In addition, according to the examination, intermediate peaks in the rising time were 56% of the maximum stress, on average.

Relatively high stresses of over 100 MPa were measured in 18 cases, of which two cases were Type II, one case was Type III, and all other cases were Type I, which is the triangle data type. In the data in which stress exceeded 100 MPa, the time variables decreased slightly compared to all data. The highest stress measured was 335.8 MPa (ship speed: 9.84 knots). Including this value, the number of values exceeding 200 MPa was four. These values were measured from 01:15 on August 29 while the bathymetric surveys were conducted. The survey detected seabed topologies in a certain area. It is thought that particularly high peak stresses were measured during the survey because even thick sea ice pieces or ice ridges could not be avoided in this case. These four data are shown separately in Fig. 6.

Table 3 Summary of characteristics of local load signals based on profile categories

Type		S_{max} (MPa)	T_r (sec)	T_{hd} (sec)	Speed (knots)
I	Max.	335.80	0.156	0.128	12.43
	Min.	50.02	0.018	0.005	0.25
	Average	72.76	0.048	0.027	7.70
II	Max.	123.04	0.292	0.181	12.85
	Min.	50.68	0.048	0.015	2.61
	Average	66.60	0.096	0.033	7.28
III	Max.	119.46	0.097	0.169	11.71
	Min.	50.24	0.018	0.021	0.91
	Average	66.85	0.052	0.055	7.41
IV	Max.	82.08	0.172	0.092	13.57
	Min.	50.04	0.068	0.015	3.45
	Average	59.52	0.110	0.050	7.63
V	Max.	76.60	0.342	0.175	10.99
	Min.	54.42	0.065	0.032	6.18
	Average	66.49	0.166	0.089	7.84
Stress over 100 MPa	Max.	335.80	0.129	0.063	11.28
	Min.	100.88	0.031	0.012	2.61
	Average	153.78	0.053	0.032	7.71
Total	Max.	335.80	0.342	0.181	13.57
	Min.	50.02	0.018	0.005	0.25
	Average	70.74	0.058	0.033	7.62

Note: S_{max}: maximum peak stress, T_r: Rising time,
T_{hd}: half decaying time, Speed: Ship speed over ground (SOG)

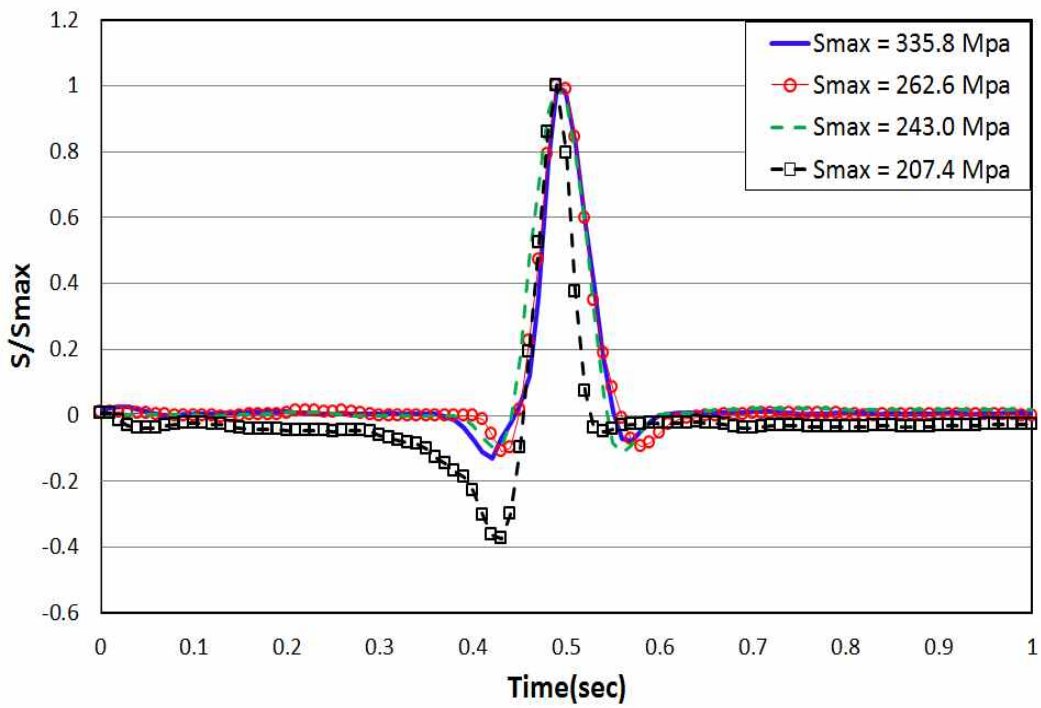

Figure 6 Comparison of the profiles of the top four related stresses

In the case of Type III, the half-decaying time showed a tendency to increase slightly because of the effects of the intermediate peaks. However, since the half-decaying time is calculated based on the point at which stress drops to 50%, compared to the maximum peak stress, the effects of the intermediate peaks appeared only when the intermediate peaks appeared in the process of the drop. Moreover, the profile should be the same as that of Type I if no intermediate peak appeared in the process. In this measurement, the stress levels were 0.5 or higher with non-dimensionalized intermediate peaks in 28 of the 35 cases.

Fig. 7 illustrates the variables of the characteristics of the data type. In this figure, the relationship between maximum peak stress and rising time is shown using all data. The figure shows that the rising time decreased, and mainly Type I data appeared when higher stresses were measured. In particular, the rising time was very short at 0.05 seconds and below. All data were Type I when stresses were higher than 150 MPa. In cases where the rising time was lengthy, many Type II, IV and V data appeared. Two cases with long rising times had Type V and Type II data.

The relationship between ship speed over ground (SOG) and rising time is shown in Fig. 8. The rising time appeared to be lengthy at ship speeds of around six knots, whereas five types of data appeared evenly in a range of ship speeds distributed between 0.25 knots (almost vessel stop state) and 13.57 knots. These results are considered to provide evidence that the data type of the ice loads acting on outer hull panels are little affected by ship speed.

Figs. 9 and 10 show the relationships among measured peak stresses, ship speed and half-decaying time. Similar to the results of the rising time, as the stress increased, the decaying time decreased, and Type I data were predominant. When the decaying time was relatively lengthy, the stress was below 100 MPa, and many Types III and IV data were found. Similar to the rising time, no tendency was found in the relationship between decaying time and ship speed.

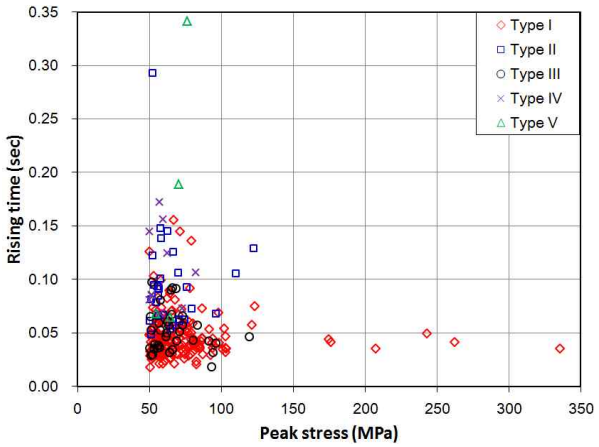

Figure 7 Relationship between stresses and rising time

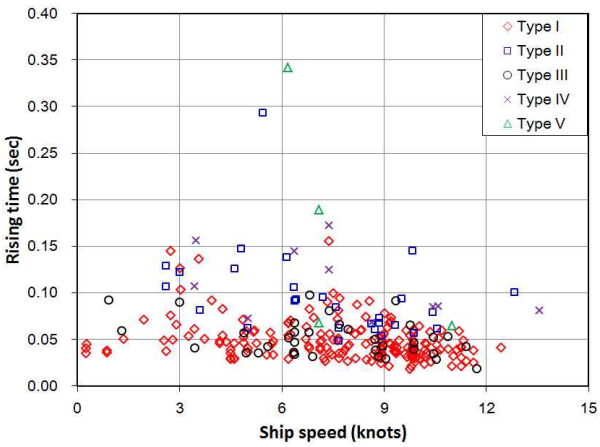

Figure 8 Relationship between ship speed and rising time

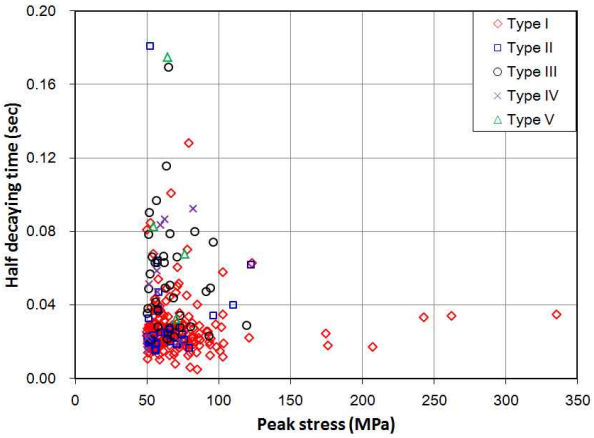

Figure 9 Relationship between stresses and half-decaying time

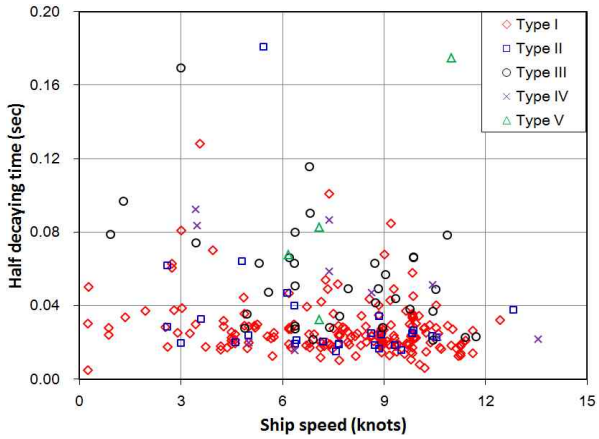

Figure 10 Relationship between ship speed and half-decaying time

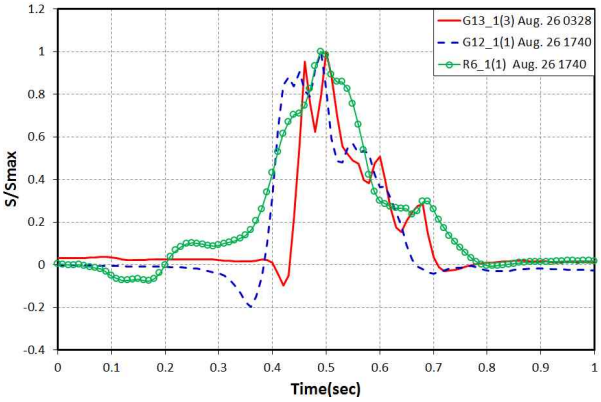

Figure 11 Example profiles of Type IV

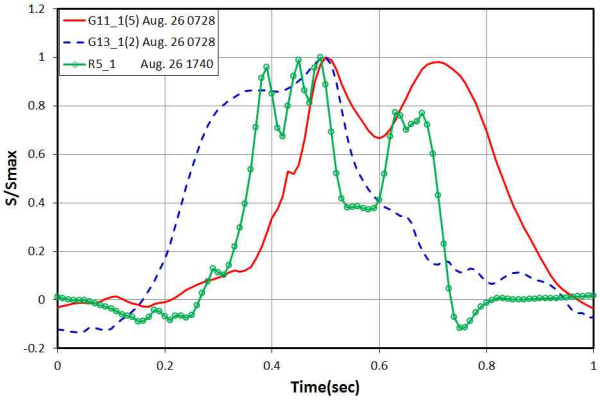

Figure 12 Example profiles of Type V

Figs. 11 and 12 show examples of dimensionless Type IV with intermediate peaks in rising and decaying periods and of Type V, a special case, respectively. Fig. 12 shows cases where two or three peaks with almost the same magnitude occurred. These cases were identified as having relatively longer rising times and longer decaying times.

Comparison with existing ice load data type

With regard to fluid impact pressure acting on hulls, according to the results of flare slamming pressure measured on large container ships sailing in the North Pacific Ocean (Lee et al., 2007), the rising times and half-decaying times were 0.116~0.282 seconds and 0.04~1.36 seconds. Wheaton et al. (1970) reported that the entire time required was within a range of 0.025~0.25 seconds during ship bottom slamming.

Frederking (1999) presented ice load data measured on the Louis S. St. Laurent, a Canadian icebreaker, while the vessel was sailing to the North Pole in the summer of 1994. The data were investigated according to the estimated ice thickness and speed (Fig. 13). To measure local ice loads, strain gauges were installed on part of the St. Laurent's hull (six frames in a 7.2 m long and 3 m high area just below the water line in the middle of the area between the stem and the bow shoulder). The time history, ice conditions, and ship speed at ice impact were recorded at the sampling rate of 100 Hz.

As shown in Fig. 13, when the ship speed was high, the force rose and dissipated quickly. When ship speed was low, long tails formed during the decaying time. In the present study, the maximum total duration of local ice load data on the Araon was calculated cumulatively from points at which time variables were the largest, at 0.704 seconds (0.342 seconds + 2 x 0.181seconds). The duration of the time variables was shown to be much longer in the case of the Canadian icebreaker although the same calculation method was used (Kwon et al., 2014). For example, when the speed was 4.0 m/s, the maximum total duration was approximately 3.8 seconds.

In addition, the figure shows that intermediate peaks appeared in almost the measured data. The reason that many intermediate peaks appeared can be inferred as the characteristics of sea ice. Sea ice floes, particularly those younger than second-year ice, are known to be considerably softer than freshwater ice. If these ice floes collide with sturdy structures such as the hulls of ship, the local shape, including the area of initial contact, may not be maintained until the maximum load, but some part of the area may be broken. Another case that may be considered is the rotation of the ice piece broken by the front of the stem while flowing backward as the ship moves forward. If the rotation occurs briefly, and if is followed by another contact, the rotation can induce an intermediate peak.

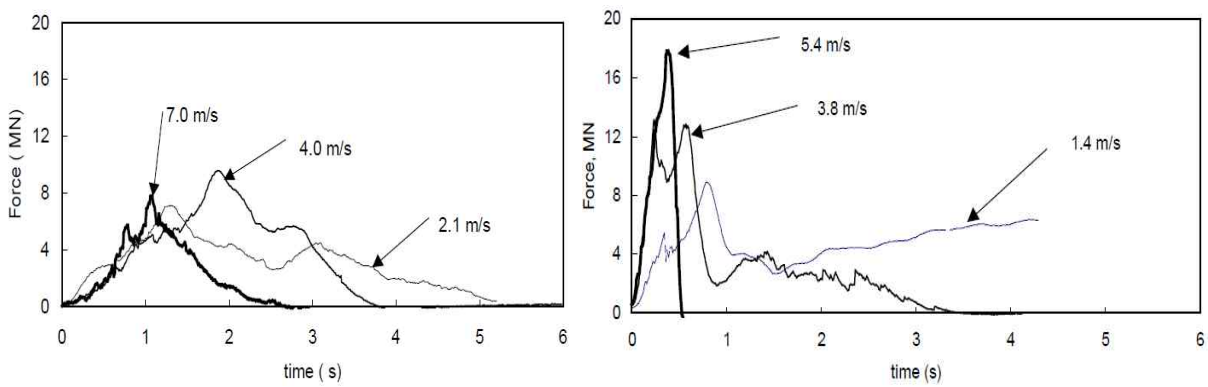

(a) On 1-2m thick ice (b) On 4-5m thick ice

Figure 13 Profiles of the Louis S. St. Laurent, glancing impact (Frederking, 1999)

In 1985, Minnick et al. (1990) conducted ice impact tests in the Beaufort Sea near Alaska using the Polar Sea, a US icebreaker. They aimed to estimate the distribution of longitudinal bending moments, and they presented representative measured strain data in the appendix of their report. Forty-one of these data were analyzed and according to the results, the rising time ranged from 0.01 seconds to 4.2 seconds (average 0.743 seconds) and the average of the rising times, excluding four cases exceeding 1.0 second, was 0.528 seconds. In addition, the half-decaying times ranged from 0.007 seconds to 1.0 seconds (average 0.2623 seconds).

Johnston et al. (2003) developed a system to estimate global ice loads from hull acceleration. They measured ice impact on the USCGC Healy and the CCGS Louis S. St. Laurent in order to identify the performance of the system. Their data were identified that the rising times of the Healy were 0.2 seconds, 0.71 seconds, and 5.7 seconds and the half-decaying times were 0.2 seconds, 0.98 seconds, and 1.9 seconds, respectively. In the case of the St. Laurent, in five impact tests, the rising times ranged from 0.31 seconds to 0.83 seconds (average 0.486 seconds), and the half-decaying times ranged from 0.155 seconds to 0.22 seconds (average 0.191 seconds). In the above data, the rising times and half-decaying times estimated in ice impact tests conducted using the Polar Sea, the Healy, and the St. Laurent were slightly longer than the time variables in the present study.

CONCLUSION

The present study attempted to analyze local ice load data measured at the side shell in the bow of the Araon, a research icebreaker, under general operation between research stations during her 2013 Arctic voyage. Only peak data of 50 MPa or higher, which are relatively high levels, were analyzed. The following conclusions are based on the findings of the present study:

(1) Two hundred and sixty-five data were analyzed and divided into five types including triangle data, which are typical fluid impact pressures. The classification criterion was whether intermediate peaks occurred or not in rising times and/or decaying times.

(2) The results of the data classification showed that Type I, triangle data, was the most frequent and accounted for approximately 70.9% of all data, followed by cases with intermediate peaks in decaying time (about 13.2%) and cases with intermediate peaks in rising times (about 10.6%). As many as 10 cases showed intermediate peaks in both durations, rising and decaying. These ratios were almost the same as those found by Kwon et al. (2014) in the Arctic voyage of the Araon in 2010.

(3) Among the measured ice load data, 18 were high stresses exceeding 100 MPa. Among these, triangle data were in the majority at 83.3%, which is almost the same ratio determined during general operation of the Arctic voyage of the Araon in 2010, which was approximately 80%. These data showed low levels of rising time and half-decaying time below 0.13 seconds and 0.007 seconds, respectively.

(4) In comparisons between maximum peak stress and rising or decaying time, as the stress increased, the rising and decaying time decreased, and Type I data with triangle shape were predominant.

(5) Comparisons between ship speeds and rising time or decaying time, showed no particular tendency. The five types of data were found evenly distributed in the entire

measurement range of the ship's speed. The present measurement was characterized by the record of 13.84 knots, which is close to the maximum sailing speed of the ship, (16 knots), and the fact that relatively high stress was identified even at a ship speed of 0.25 knots, a state in which the ship is almost a standstill.

ACKNOWLEDGEMENT

This research was supported by the BK21 Plus project. The authors gratefully acknowledge this support.

REFERENCES

ABS, 2011. Guide for Ice Load Monitoring System, American Bureau of Shipping, Houston, TX, USA.

Cuomo, G., Lupoi, G., Shimosako, K., and Takahashi, S. 2011. Dynamic response and sliding distance of composite breakwaters under breaking and non- breaking wave attack, Coastal Engineering, Vol. 58, pp. 953-969.

Frederking, R., 1999. The Local Pressure-Area Relation in Ship Impact with Ice, Proc. 15th International Conference on Port and Ocean Engineering under Arctic Conditions (POAC'99), Vol. 2, pp. 687-696, Helsinki, Finland, August 23-27.

Gagnon, R.E. and Wang, J., 2012. Numerical simulations of a tanker collision with a bergy bit incorporating hydrodynamics, a validated ice model and damage to the vessel, Cold Regions Science and Technology, Vol. 81, pp. 26-35.

Goda, Y., 1994. Dynamic response of up-right breakwater to impulsive force of breaking waves, special issue on vertical breakwaters, Coastal Engineering, Vol. 22, pp. 135-158.

ISSC, 2012. Arctic Technology, International Ship and offshore Structures Congress (ISSC), Committee V.6 report.

Jeon, Y.J., Rim, C.W. and Lee, T.K., 2013. Profile Analysis on Signal Measured Local Ice Load during Icebreaking in Arctic Sea, J. Navig. Port Res., Vol. 37, No. 2, pp. 143-148.

Johnston, M., Frederking, R., Timco, G., Miles, M., 2003. Ice-Induced Global Loads on USCGC HEALY and CCGS LOUIS S. ST. LAURENT as Determined from Whole-ship Motions, National Research Council Canada, Technical Report CHC (Canadian Hydraulics Centre)-TR-014.

Kim, H.S. Lee, C.J. Choi, K.S. & Kim, M.C., 2011. Study on Icebreaking Performance of the Korea Icebreaker ARAON in the Arctic Sea, International Journal of Naval Architecture and Ocean Engineering, 3, pp. 208-215.

Kwon, Y.H., Jeon, Y.J., Rim, C.W., Lee, T.K., 2014. Characteristics analysis of local ice load signals in ice-covered waters, The 28th Asian-Pacific Technical Exchange and Advisory Meeting on Marine Structures (TEAM 2014), Istanbul, Turkey, 13-16 October.

Lee, T.K., Rim, C.W., Kim, Y.N., Heo, J.H. and Kim, B.H., 2007. A Study on Measurement of Flare Slamming of Large Container Vessel (II) -Characteristic Analysis of Measured Slamming Pressure-, J. of the Society of Naval Architects of Korea, Vol. 44, No. 3, pp. 279-284.

Lee, T.K., Kim, T.W., Rim, C.W. and Kim, H.S., 2014. A Study on Analysis of Ice Load Measured during the Voyage in the Arctic Sea, J. of the Society of Naval Architects of Korea, Vol. 51, No. 2, pp. 107-113.

Lundgren, H., 1969. Wave shock forces: an analysis of deformations and forces in the wave and in the foundation, Proc. Symp. on Research in Wave Action, Delft Hydraulics Lab., Delft, The Netherlands, pp. 1-20.

Minnick, P., St. John, J., Cowper, B., Edgecombe, M., 1990. Global Ice Forces and Ship Response to Ice, Ship Structure Committee, Report No. SSC-341.

Oumeraci, H. and Kortenhaus, A., 1994. Analysis of dynamic response of caisson breakwaters, special issue on vertical breakwaters, Coastal Engineering, Vol. 22, pp. 159-183.

Oumeraci, H., Kortenhaus, A., Allsop, N. W. H., De Groot, M. B., Crouch, R. S., Vrijling, J. K., Voortman, H. G., 2001. Probabilistic Design Tools for Vertical Breakwaters, Balkema, Rotterdam.

Paik, J.K., Chung, J.Y. and Paik, Y.M., 1999. A Study on the Collapse Strength Characteristics of Ship Bottom Plating Subject to Slamming Induced Impact Lateral Pressure Loads, J. of the Society of Naval Architects of Korea, Vol. 36, No. 2, pp. 77-93.

Republic of Liberia, 2009. Decision of the Commissioner of Maritime Affairs, R.L. and the Report of Investigation in the Matter of Sinking of Passenger Vessel EXPLORER (O.N. 8495), 23 November 2007 in the Bransfield Strait near the South Shetland Islands. Published by the Bureau of Maritime Affairs, Monrovia, Liberia. 26 March.

Shimosako, K., Takahashi, S. and Tanimoto, K., 1994. Estimating the sliding distance of composite breakwaters due to wave forces inclusive of impulsive forces, Proc. of 24th Int. Conf. Coastal Eng., ASCE, Kobe, pp. 1580-1594.

Shimosako, K. and Takahashi, S., 1999. Application of deformation-based reliability design for coastal structures, Proc. of Coastal Structures, Vol. I, Balkema, Santander, Spain, pp. 363-371.

Wheaton, J.W., Kano, C.H., Diamant, P.T. and Bailey, F.C., 1970. Analysis of slamming data from the S.S. Wolverine State, Ship Structure Committee, Report No. SSC-210.